

Portland State University

PDXScholar

---

Chemistry Faculty Publications and  
Presentations

Chemistry

---

10-25-2006

# Fermiology and superconductivity at high magnetic fields in a completely organic cation radical salt

J. S. Brooks

V. Williams


E. Choi

D. Graf

M. Tokumoto

*See next page for additional authors*

Follow this and additional works at: [https://pdxscholar.library.pdx.edu/chem\\_fac](https://pdxscholar.library.pdx.edu/chem_fac)

 Part of the [Atomic, Molecular and Optical Physics Commons](#)

Let us know how access to this document benefits you.

---

## Citation Details

J.S. Brooks, V. Williams, E. Choi, D. Graf, M. Tokumoto, S. Uji, F. Zuo, J. Wosnitza, J. Schlueter, H.D. Davis and R. Winter, "Fermiology and Superconductivity at High-Magnetic Fields in a Completely Organic Charge Transfer Complex," *New Journal of Physics*, 8, 255 (2006).

This Article is brought to you for free and open access. It has been accepted for inclusion in Chemistry Faculty Publications and Presentations by an authorized administrator of PDXScholar. Please contact us if we can make this document more accessible: [pdxscholar@pdx.edu](mailto:pdxscholar@pdx.edu).

---

**Authors**

J. S. Brooks, V. Williams, E. Choi, D. Graf, M. Tokumoto, S. Uji, F. Zuo, J. Wosnitza, J. A. Schlueter, H. David, Rolf Walter Winter, Gary L. Gard, and K. Storr

## Fermiology and superconductivity at high magnetic fields in a completely organic cation radical salt

J S Brooks<sup>1</sup>, V Williams<sup>1</sup>, E Choi<sup>1</sup>, D Graf<sup>1</sup>, M Tokumoto<sup>2</sup>, S Uji<sup>3</sup>, F Zuo<sup>4</sup>, J Wosnitza<sup>5</sup>, J A Schlueter<sup>6</sup>, H Davis<sup>7</sup>, R W Winter<sup>7</sup>, G L Gard<sup>7</sup> and K Storr<sup>1,8</sup>

<sup>1</sup> Physics Department and NHMFL, Florida State University, Tallahassee, FL 32310, USA

<sup>2</sup> Nanotechnology Research Institute, AIST, Tsukuba, Ibaraki 305-8568, Japan

<sup>3</sup> National Institute for Materials Science, Sakura, Tsukuba, Ibaraki 305-0003, Japan

<sup>4</sup> Department of Physics, University of Miami, Coral Gables, FL 33124, USA

<sup>5</sup> Hochfeld-Magnetlabor Dresden (HLD), Forschungszentrum Rossendorf, D-01314 Dresden, Germany

<sup>6</sup> Materials Science Division, Argonne National Laboratory, Argonne, IL 60439, USA

<sup>7</sup> Department of Chemistry, Portland State University, Portland, OR 97207, USA

<sup>8</sup> Department of Physics, Prairie View A&M University, Prairie View, TX 77446, USA

E-mail: [brooks@magnet.fsu.edu](mailto:brooks@magnet.fsu.edu)

*New Journal of Physics* **8** (2006) 255

Received 1 August 2006

Published 25 October 2006

Online at <http://www.njp.org/>

doi:10.1088/1367-2630/8/10/255

**Abstract.** We report specialized interplane magnetoresistance (MR) measurements on the organic superconducting compound  $\beta''$ -(BEDT-TTF)<sub>2</sub>SF<sub>5</sub>CH<sub>2</sub>CF<sub>2</sub>SO<sub>3</sub> (where BEDT-TTF is bis(ethylenedithio)tetrathiafulvalene) in both the superconducting ( $T_c \sim 5$  K) and normal states versus magnetic field direction. In the normal state, detailed angular-dependent magnetoresistance oscillation (AMRO) studies reveal peculiar features of the Fermi surface topology of this compound, and very high magnetic field studies further support the unusual nature of the electronic structure. In the superconducting state we investigate, through detailed AMRO measurements, the

anomalous MR peak that appears within the superconducting field-temperature phase diagram. Our results reveal a direct connection between the superconducting state determined from purely in-plane field, and the vortex lattice produced by the inter-plane magnetic field. We also describe several unique sample rotation instruments used in these high field experiments, including the use of dysprosium pole pieces in combination with a 45 T hybrid magnet to carry out measurements at the highest steady-state resistive magnetic field (47.8 T) yet achieved.

## Contents

<b>1. Introduction</b>	<b>2</b>
<b>2. Experimental methods and results</b>	<b>4</b>
2.1. High field MR and AMRO measurements . . . . .	4
2.2. Continuous $\theta - \phi$ AMRO measurements . . . . .	8
2.3. AMRO in the superconducting critical region. . . . .	12
<b>3. Discussion and summary</b>	<b>17</b>
3.1. Very high field measurements . . . . .	17
3.2. Highly systematic AMRO studies . . . . .	18
3.3. Interplane transport in the superconducting critical region . . . . .	19
<b>4. Conclusions</b>	<b>19</b>
<b>Acknowledgments</b>	<b>20</b>
<b>References</b>	<b>20</b>

## 1. Introduction

In this paper, we focus on the superconducting and normal state properties of the organic charge transfer salt  $\beta''$ -(BEDT-TTF)<sub>2</sub>SF<sub>5</sub>CH<sub>2</sub>CF<sub>2</sub>SO<sub>3</sub> [1], as explored by detailed angular-dependent magnetoresistance oscillation (AMRO) and high magnetic field measurements. This particular type of organic charge transfer salt is unusual in that both the electron donor molecule, BEDT-TTF, and the anion, SF<sub>5</sub>CH<sub>2</sub>CF<sub>2</sub>SO<sub>3</sub><sup>-</sup>, are organic. Equally unique is the low symmetry nature of the anion, and the less common  $\beta''$  stacking motif of the donor molecules. Physical and electronic structural aspects of the material are shown in figure 1.

Some of the unusual physical properties of this material, to be further addressed in the present study, are:

### 1. Fermiology

Band structure calculations [2] predict a single closed orbit and open orbit sheets (figure 1(c)). Shubnikov-de Haas (SdH) and de Haas–van Alphen (dHvA) measurements [3] give extremal orbits that are considerably smaller than the predicted orbit size which is expected to be about 14.8% of the FBZ. Likewise, AMRO studies, which yield a description of the in-plane, azimuthal dependence of the Fermi momentum  $k_F(\phi)$  [4]–[6], indicate a much more elliptical orbit than described in figure 1(c) [3]. Specifically,

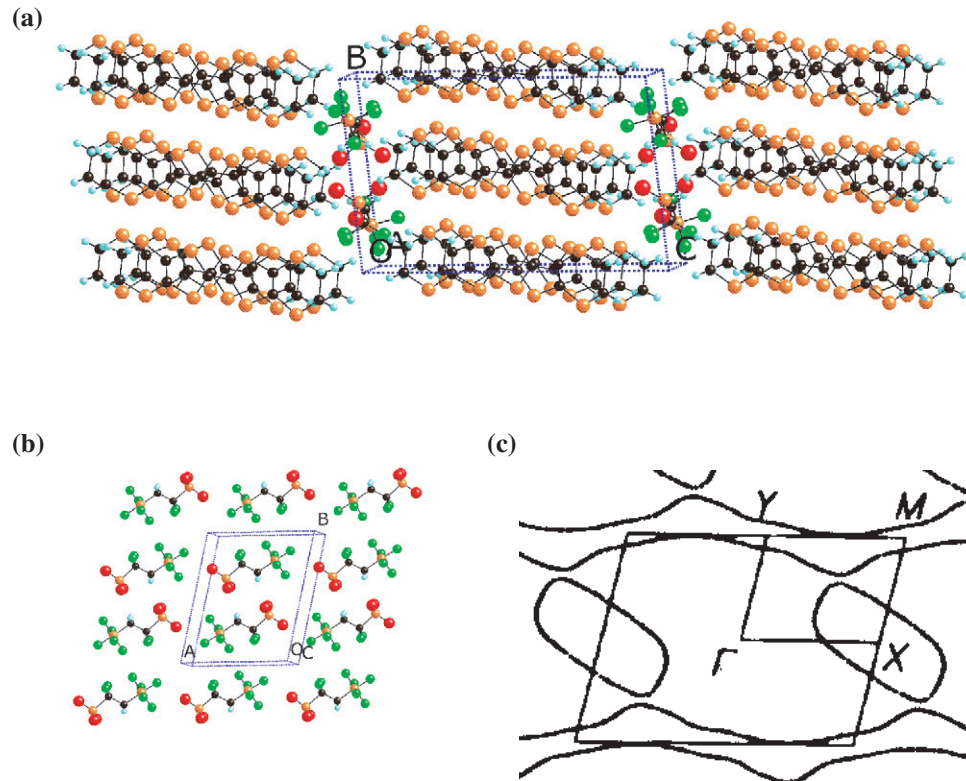


**Figure 1.**  $\beta''$ -(BEDT-TTF) $_2$ SF $_5$ CH $_2$ CF $_2$ SO $_3$  (a) Packing diagram. The BEDT-TTF stacking direction is along the  $a$ -axis direction (normal to the page). The unit cell parameters at  $T = 123$  K are  $a = 9.1536(6)$  Å,  $b = 11.4395(8)$  Å,  $c = 17.4905(12)$  Å [1]. Colour code: sulphur (orange), carbon (black), hydrogen (blue), oxygen (red) and fluorine (green). (b) Packing diagram of the SF $_5$ CH $_2$ CF $_2$ SO $_3^-$  layer. (c) Fermi surface (FS) topology derived from double zeta band structure calculations [2]. Here  $\Gamma = (0, 0)$ ,  $Y = (0, k_b/2)$ , and  $X = (k_a/2, 0)$ . The computed area of the hole pockets is about 14.8% of the first Brillouin zone (FBZ).

the FBZ area is  $0.377$  Å $^{-2}$ , the quantum oscillation area from SdH and/or dHvA is  $\sim 200$  T (or  $0.0192$  Å $^{-2} = 5\%$  of the FBZ), and the AMRO yields  $0.0194$  Å $^{-2}$ .

## 2. Quantum oscillations

Wosnitza *et al* [7] (and earlier Zuo *et al* [8]) have made extensive MR measurements on this material. They find that in addition to the SdH oscillations indicative of metallic behaviour, there is an additional background MR that increases with increasing field and lower temperatures i.e., the background MR exhibits field-induced metal-insulator behaviour. By taking into account the background MR and computing the oscillatory conductivity from the data, good agreement can be found between the SdH data and complementary magnetization (dHvA) waveforms measured independently. (An alternative interpretation involves a thermal activation mechanism between Landau levels [9].)

### 3. Superconductivity

Another unusual aspect of the MR in  $\beta''$ -(BEDT-TTF)<sub>2</sub>SF<sub>5</sub>CH<sub>2</sub>CF<sub>2</sub>SO<sub>3</sub> occurs at the superconducting critical field transition where a peak in the MR is observed in the vicinity of  $B_{c2}$  for field and current perpendicular to the conducting layers ( $B \parallel c$  and  $I \parallel c$ ) [10]. This peak effect, which is found in a number of low dimensional superconductors, is thought to arise from dissipation in the Abrikosov vortex lattice structure caused by a decrease in interplanar Josephson tunnelling near the critical phase boundary [10]–[14].

In the study reported here, we take a closer look at some of these anomalous aspects of the compound through high field transport measurements and detailed AMRO studies in both the normal and superconducting states. We find that the metal-insulator behaviour seen in the background MR continues to 45 T; that the AMRO, normally dominated at low-fields by oscillations due to commensurate FS effects [15], is instead dominated at 45 T by SdH oscillations with very high amplitudes at 45 T; that detailed two-angle AMRO at lower fields shows an anomaly along certain crystallographic directions; and that MR in the superconducting critical field region shows unambiguously that the peak anomaly near  $B_{c2}$  is indeed related to the Abrikosov vortex lattice induced only by magnetic fields perpendicular to the conducting layers.

## 2. Experimental methods and results

The single crystal of  $\beta''$ -(BEDT-TTF)<sub>2</sub>SF<sub>5</sub>CH<sub>2</sub>CF<sub>2</sub>SO<sub>3</sub> used in this study was prepared by electrochemical methods [1] and the crystallographic alignment was checked by x-ray diffraction. Resistance measurements were carried out for current applied parallel to the  $c$ -axis direction (interplane transport) using a standard four-terminal constant current ac configuration typically in the 10–100  $\mu$ A range. Earlier results involving an angular-dependent investigation of the same crystal using a two-angle rotation system in a 14 T magnet at the National Institute for Materials Science, Tsukuba, Japan have been previously published [16], and some additional study from that study is reported herein. In the present study, we focus on high field study carried out in the 45 T Hybrid magnet [17]–[19] at the National High Magnetic Field Laboratory (NHMFL), Tallahassee, USA, more detailed two-angle AMRO studies carried out in a 18 T superconducting magnet at the NHMFL, and MR studies in the superconducting state carried out in a single-angle rotation system in a 9 T superconducting magnet at the Nanotechnology Research Institute (AIST), Tsukuba, Japan.

### 2.1. High field MR and AMRO measurements

For the 45 T experiment, a special rotation platform was built that operated at helium-three temperatures within the poles of a dysprosium field enhancement stage [20, 21], as shown in figure 2. At low temperatures, the magnetization field  $B_{\text{sat}}$  of Dy saturates to a value of  $\sim 2.8$  T at applied fields less than 0.5 T at low temperatures [20], and in the present measurements, we report the saturated field  $B_{\text{tot}} = B_{\text{applied}} + B_{\text{sat}}$ , where  $B_{\text{tot}}$  reaches 47.8 T when the Hybrid is at full field.

Representative data is shown in figure 3 for  $\beta''$ -(BEDT-TTF)<sub>2</sub>SF<sub>5</sub>CH<sub>2</sub>CF<sub>2</sub>SO<sub>3</sub> at 0.9 K for  $I \parallel c$  and  $B \parallel c$ . For the field sweep data in figure 3(a), full superconductivity is observed below a field of about 3 T, although the details of the MR in this range are complicated by the rapid

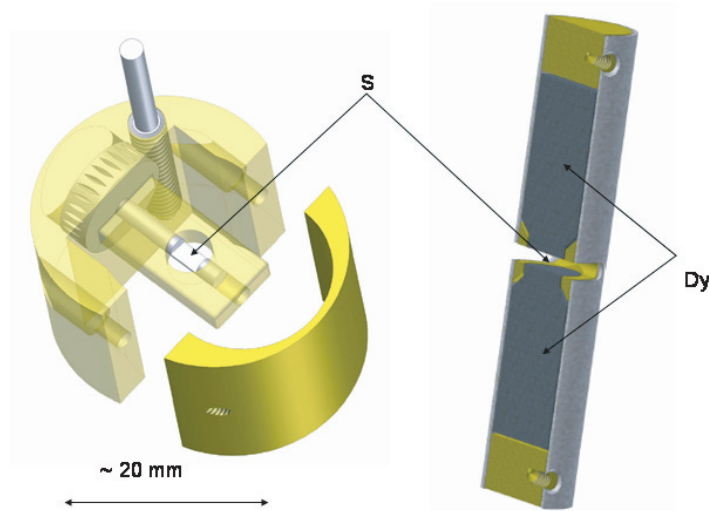


**Figure 2.** Dysprosium field-enhanced sample rotation stage. Left image: rotation assembly (brass with stainless steel shafts and set screws). Here the sample is placed at position S on a flat portion of the rotation axle, and sample leads are fed out through an axial clearance hole. Right image: vertical cross-section (along the field direction) of the two Dy pole pieces. The poles are held in place inside a stainless steel tube with brass end caps and a central spacer with a rectangular clearance for access to the pole gaps. The tongue of the rotation stage is inserted into the clearance gap, and the rotation stage is secured to the Dy pole assembly by a semi-cylindrical clamp. The sample is positioned centrally and rotates through  $360^\circ$  between the 1.5 mm gap of the Dy pole pieces.

saturation of the Dy pole pieces. Nevertheless, the anomalous MR peak, to be discussed in more detail below, is clearly observed. At higher fields, the quantum oscillations associated with the 200 T SdH frequency are apparent, as is a rise in the background MR. In figure 3(b), the AMRO at 47.8 T is presented for a complete rotation of the polar angle  $\theta$  through  $360^\circ$ . (We note that this experiment took 1 h, and that 47.8 T was maintained for the entire period. To our knowledge, this is the highest dc magnetic field experiment yet performed).

The high field measurements confirm the appearance of the anomalous background MR that increases with magnetic field [7, 8]. By determining  $R_B(B)$  (the background MR from either the peaks or valleys of the SdH waveforms), and using the standard prescription to compute the oscillatory conductivity  $\sigma_{\text{osc}} = [(R(B) - R_B(B))/R_B(B)]^{-1}$ , we can reproduce the essential features in  $\sigma_{\text{osc}}$  complementary to the magnetization signal [7] as shown in figure 4, including the asymmetry of the wave forms. The presence of the background MR and its implications for metal-insulator behaviour are the first indication that the details of the electronic structure of this compound are not yet well understood.

The AMRO measurements performed at 47.8 T in figure 3(b) reveal the appearance of SdH oscillations to much higher angles than standard low-field studies. In contrast, the AMRO described below, are greatly obscured in the data. Comparisons between the SdH and AMRO behaviour are presented in figure 5. Some remarkable features of the SdH oscillations include their very high amplitude at large angles where the spin damping term [22] would otherwise make



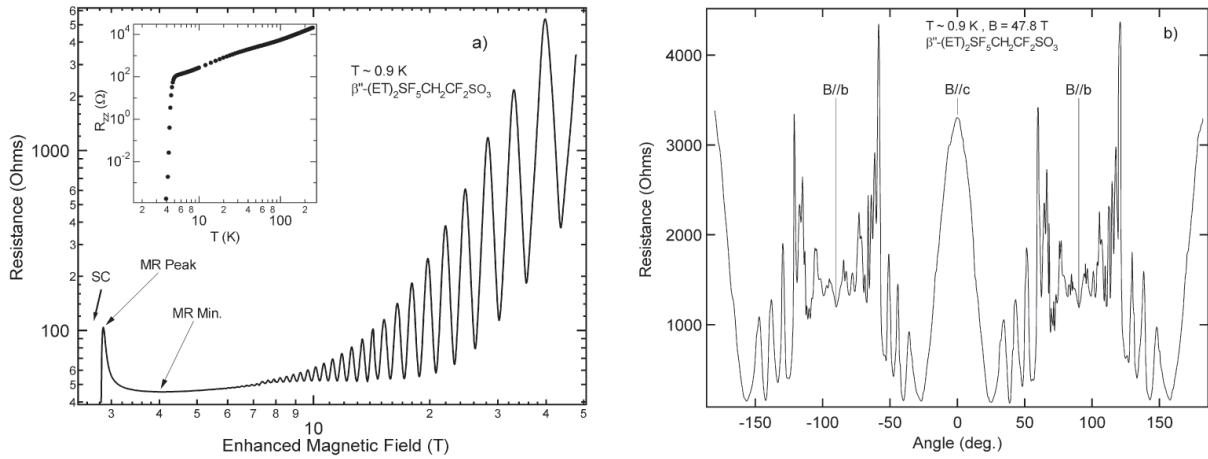


**Figure 3.** (a) Complete field sweep for  $\beta''$ -(BEDT-TTF) $_2$ SF $_5$ CH $_2$ CF $_2$ SO $_3$  in the hybrid magnet for  $B \parallel c$  and (inset) inter-planar resistance versus temperature at zero magnetic field. Note log–log scales. The outsert superconducting magnet is first energized. Here, below about 0.2 T, the Dy saturates to 2.8 T quickly, and the sample goes from the superconducting state into the region of the MR peak. At higher fields the MR goes through a minimum, and then increases and the SdH oscillations appear. When the superconducting outsert reaches the final background field of 12 T, the resistive insert magnet is then swept up to its full field of 33 T, and with the Dy enhancement, 47.8 T is ultimately reached. (b) AMRO of  $\beta''$ -(BEDT-TTF) $_2$ SF $_5$ CH $_2$ CF $_2$ SO $_3$  at 47.8 T. The data is for a complete 360° rotation of the polar angle  $\theta$  for a fixed azimuthal angle of  $\phi \sim 10^\circ$  away from the  $b$ -axis towards the  $a$ -axis in the  $a$ – $b$  plane.

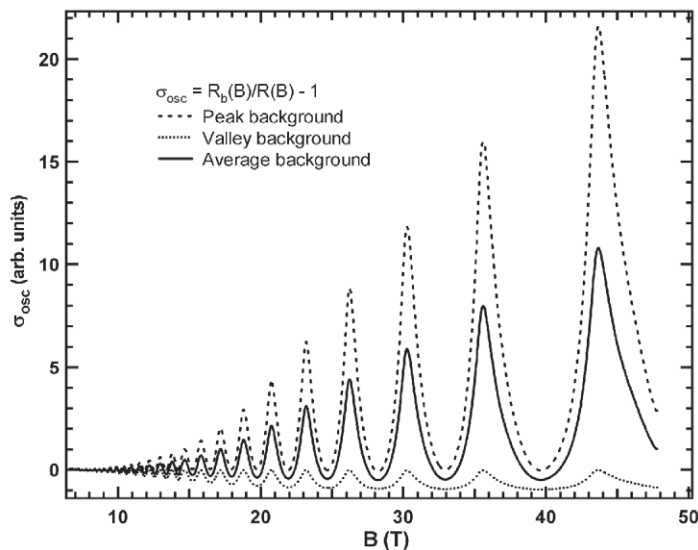


**Figure 4.** Oscillatory conductivity of  $\beta''$ -(BEDT-TTF) $_2$ SF $_5$ CH $_2$ CF $_2$ SO $_3$  for  $B \parallel c$  and  $T = 0.9$  K. The data are presented for evaluation of the background MR from the peaks, valleys, or their average obtained from figure 3(a).



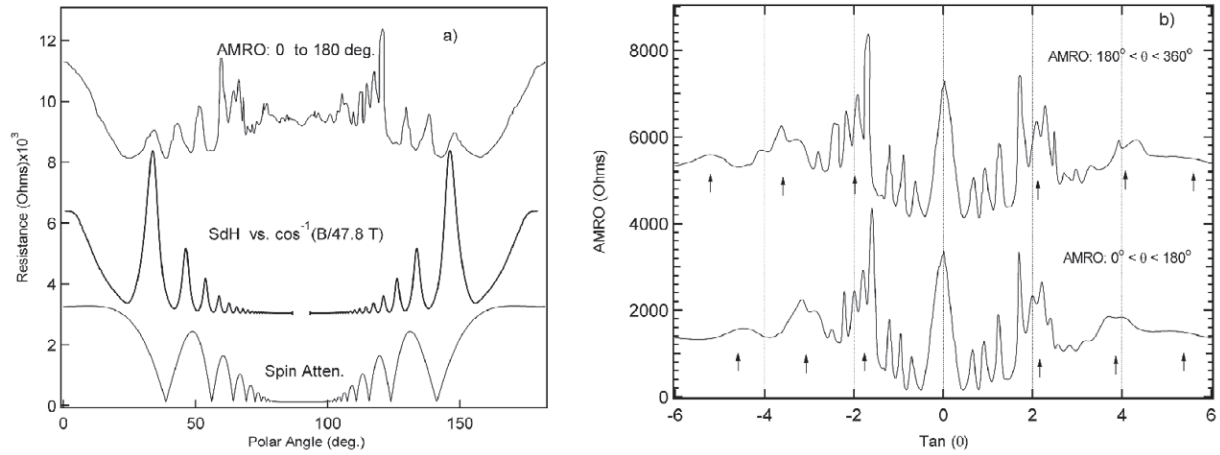


**Figure 5.** (a) Comparison of the magnetoresistance signal at 47.8 T versus polar angle  $\theta$  with the signal expected from the SdH oscillations solely from the field component perpendicular to the  $a$ - $b$  plane (derived from figure 3(a)). Also shown is the expected modulation of the SdH amplitude versus  $\theta$  from the SA term (from [3]) Traces are offset for clarity, and the SA trace is in arbitrary units. (b) AMRO data for two consecutive 180° scans versus  $\tan(\theta)$ . Approximate location of AMRO peaks is indicated by arrowheads. Upper trace is offset for clarity. Although the accompanying SdH oscillations are complex, their behaviour is reproducible for the two consecutive 180° rotations.

them significantly smaller. Likewise, the correspondence between SdH oscillations obtained by sample rotation with  $B_0 \cos(\theta)$  where  $B_0 = 47.8$  T, and those obtained for field sweeps up to 47.8 T with  $B \parallel c$  was not systematic.

The formalism used to describe the AMRO measurements involves the following basic relationships. In reference to figure 1(c) for instance, a sample rotated in a constant magnetic field is achieved where the polar angle  $\theta$  is defined as the angle between the field and the  $c$ -axis. In addition, the azimuthal angle  $\phi$  defines the direction of rotation of the field with respect to the  $a$ - $b$  plane. Due to the warped cylindrical nature of the hole orbits in layered materials [15], the interplane MR will oscillate periodically with  $\tan(\theta)$  according to

$$\tan(\theta_n) \sim \pi(n \pm 1/4)/k_{B \max} c, \quad (1)$$

where we consider only interplane hopping of the carriers [6, 23]. There will be maxima in the interplane MR  $R_{zz}$  associated with integers  $n = \pm 1, 2, 3, \dots$  that appear with period  $\Delta \tan(\theta) = \tan(\theta_n) - \tan(\theta_{n-1})$  (where we note that there is a  $\pi/4$  phase shift upon crossing  $\theta = 0$ ). For a strictly circular orbit,  $k_{B \max}$  will be the  $k_F$ , and hence  $k_F = \pi/c \Delta \tan(\theta)$ . For non-circular orbits as in figure 1(b) where the  $k_F$  is a function of azimuthal angle, i.e.  $k_F(\phi)$ , a geometrical construction is used to construct  $k_F(\phi)$  from  $k_{B \max}(\phi)$  [6, 23], where it is noted that the more elliptical the real  $k_F(\phi)$  orbit becomes, the more ‘peanut-like’  $k_{B \max}(\phi)$  appears [3, 24].

Since at high magnetic fields the SdH oscillations can also be present, additional features in the MR will appear, especially in quasi-two dimensional (2D) (cylindrical FS) systems as in the case of the title material. In this case the component of the field parallel to the cylindrical

FS, which produces the SdH signal, will change with angle as  $B \parallel c = B_0 \cos(\theta)$ . Hence, as discussed above, a rotation of  $\theta$  from 0 to  $90^\circ$  is like sweeping the  $B \parallel c$  field from  $B_0$  to 0, and this will produce SdH oscillations. The middle trace in figure 5(a) represents the anticipated result of rotation based on figure 3(a), assuming no other effects. However, since there is a difference between the orbital Landau level spacing and the Zeeman spin splitting, an additional spin attenuation (SA) factor arises, comprising the temperature, Dingle, and spin-zero terms, which modulates with  $\theta$  the amplitude of the fundamental SdH amplitude [2]:

$$SA \sim \exp(-\alpha\mu_c(\theta)(T + T_D)/B) |\cos(\pi g\mu_b(\theta)/c)| / \cos(\theta). \quad (2)$$

Here the cyclotron mass  $\mu_c$  and the product of the  $g$ -factor and the effective mass  $g\mu_b$  are both proportional to  $1/\cos(\theta)$ . (This reduction factor is shown in the lower trace of figure 5(a)). The effect of the SA term is to diminish, in a periodic manner, the SdH amplitudes as the field is rotated away from  $B \parallel c$ . Although the SdH amplitudes at first attenuate as expected with the spin-zero amplitude, the amplitudes at large angles become very large. Moreover, the direct correspondence between the SdH peak positions from the field sweep and rotation data breaks down almost immediately as the field is rotated away from  $B \parallel c$ . The apparent anomalous behaviour of the SdH oscillations (i.e. the large amplitudes and the difference of the SdH peaks for comparable  $B \parallel c$  and  $B \cos(\theta)$  values) may result from other factors we have not here taken into account, such a more complete inclusion of the angular dependence of the Lifshitz–Kosevich attenuation factors [22], and the influences of the AMRO background and MR background. A more extensive experimental and analytical treatment will be needed to sort out the details.

The AMRO oscillations (periodic in  $\tan(\theta)$  as shown in figure 5(b)) are apparent, but significantly obscured by the much larger SdH signal in the data. Because the plane of rotation is near the  $b$ – $c$  plane, the AMRO appear at large values of  $\tan(\theta)$ , where the uncertainties become greater. Following equation (1), the approximate period is  $\Delta \tan(\theta) \sim 2$  which corresponds to  $k_{B_{\max}} \sim 0.09 \text{ \AA}^{-1}$ . As we will discuss in the next section, the AMRO period near the  $b$ – $c$  plane is also anomalous.

## 2.2. Continuous $\theta - \phi$ AMRO measurements

In high field magnets and at cryogenic temperature, continuous multiple angle rotations become more challenging. For the 50 mm bore 31 T resistive and 20 T superconducting magnet systems at the NHMFL, we designed a unique rotation system as shown in figure 6. The essential feature of the design is that for every  $360^\circ$  rotation of the sample with polar angle  $\theta$ , the sample platform also rotates about its orthogonal azimuthal axis by  $6.92^\circ$ . The latter is accomplished by meshing the 52-tooth gear on the perimeter of the sample holder with the threaded, fixed axle of the rotator. Through the use of either sliding contacts, or by spooling twisted pair leads on to the rotator body, continuous rotations of both  $\theta$  and  $\phi$  could be carried out using a single rotation shaft (driven by a stepper motor) until a complete  $2\pi$  rotation of both angles could be accomplished. Representative data for  $\beta''$ -(BEDT-TTF) $_2$ SF $_5$ CH $_2$ CF $_2$ SO $_3$  carried out at 1.5 K and 10 T in a superconducting magnet is shown in figure 7.

To prepare the data set shown in figure 7 for analysis, it was useful to determine the position of each of the superconducting minima that appeared whenever the field was exactly in-plane. Because the sample was only partially superconducting at the field and temperature of the measurement, this was a very sharp and precise feature. (Even when the sample is not

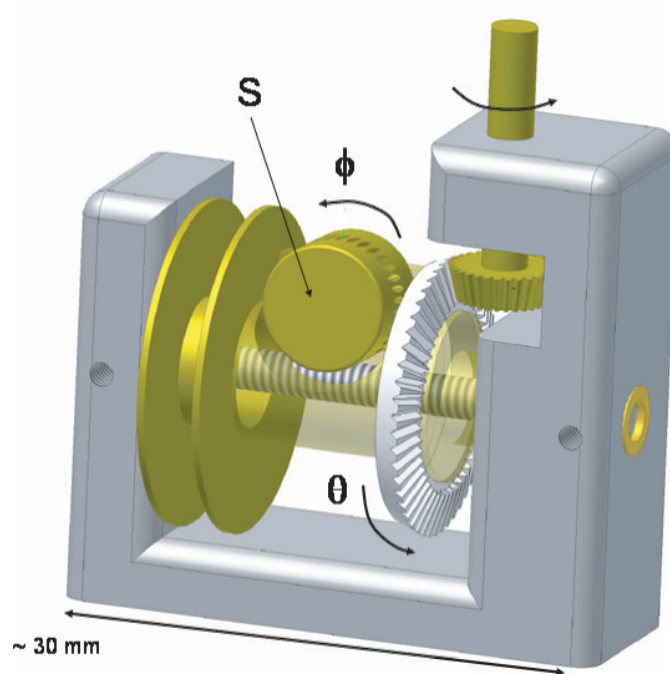


**Figure 6.** (a) Rotation assembly for continuous  $\theta - \phi$  MR measurements. A single shaft from room temperature operates the main  $\theta$ -rotation motion of the sample platform assembly. The 52-gear tooth sample platform (S) is meshed with threaded axis that is clamped to the body of the assembly; for every  $360^\circ$  rotation of the main rotator body, the sample platform advances continuously in  $\phi$  by  $6.92^\circ$ . The central axis and set screws are non-magnetic stainless steel. The body of the rotator and all gearing is made of brass. Twisted pair cabling is drawn from a supply spool on to the shaft spool to allow continuous electrical four-terminal contact to the sample. Sliding graphite contacts have also been used for continuous sample electrical contact during rotations.

superconducting, a peak or valley feature is generally observed for the in-plane field orientation—see the  $B \parallel a-b$  points in figure 3.) Since there is always uncertainty in placing the sample with the  $a-b$  plane exactly parallel to the sample platform, a comparison of the position of the superconducting minima with respect to the digital stepper count produced an alignment error signal (‘dither’) that was taken into account in the analysis, as shown in figure 8(a). This measurement also allowed the determination of the azimuthal dependence of the MR in the exact in-plane critical field region for this temperature and field, as shown in figure 8(b).

Comparisons of the experimental data with the results expected from the computed FS are shown in figures 9 and 10. The results associated with equation (1) are presented in figure 9(b), where the value  $k_{B \max}$  is plotted versus azimuthal angle  $\phi$ . To produce these results, the data was Fourier transformed with respect to  $\tan(\theta)$  for each interval of  $\theta = \pi$  to obtain the period in  $\tan(\theta)$ . The intervals of  $\phi$  are  $\sim 3.46^\circ$  since  $\phi$  changes by this amount for each  $\pi$  interval of  $\theta$ . We note that although the standard ‘peanut’ pattern characteristic of an elliptical orbit is obtained, there appears to be a discontinuity to a second behaviour for field rotations in the azimuthal plane between the  $b$  and  $c$  directions. In figure 10(a), the predicted AMRO

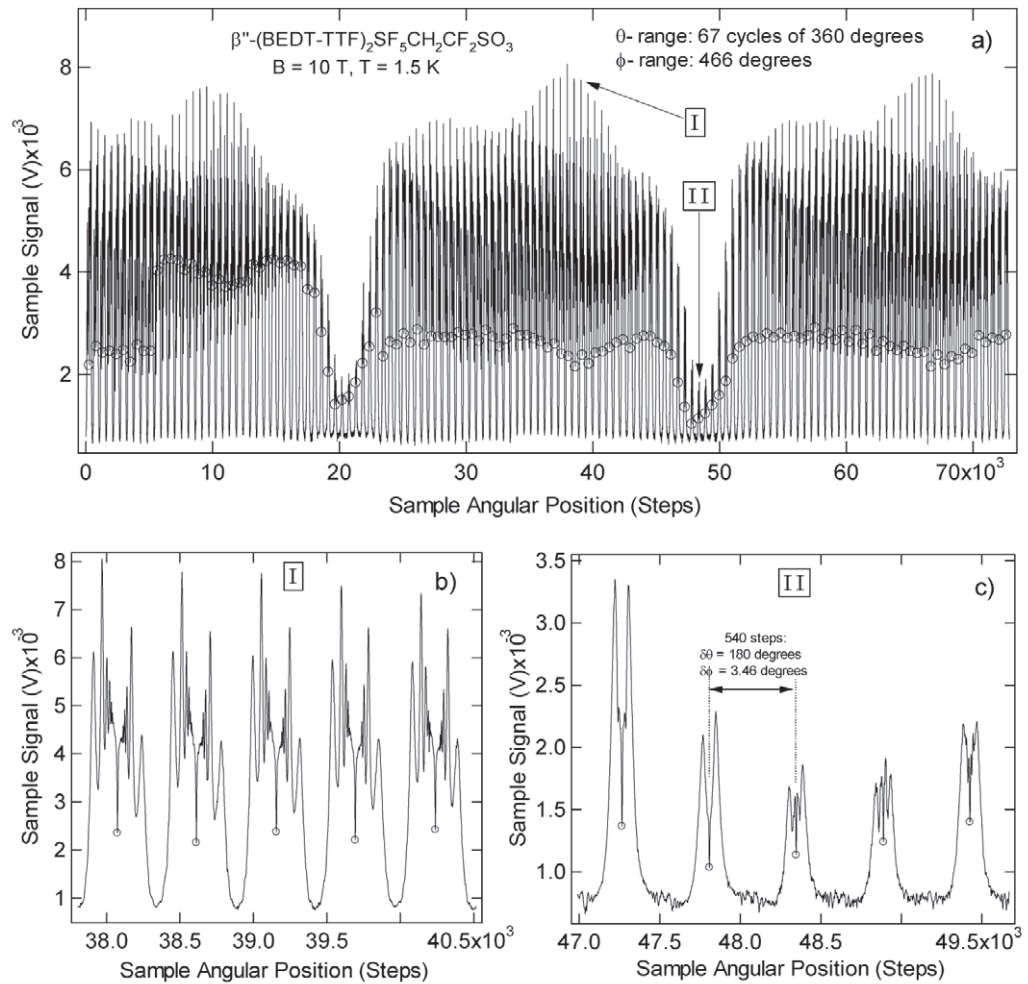


**Figure 7.** (a) Interplane voltage signal ( $I \parallel c$ ) for a continuous  $\theta - \phi$  rotation of  $\beta''$ -(BEDT-TTF)<sub>2</sub>SF<sub>5</sub>CH<sub>2</sub>CF<sub>2</sub>SO<sub>3</sub> at 10 T and 1.5 K. ‘o’—position of minima for  $\theta$  modulo  $90^\circ$  ( $B \parallel a-b$  plane) where the sample becomes partially superconducting. (Note that first 5000 steps were at a lower temperature of  $\sim 1.3$  K.) Panels (b) and (c) are details of regions I and II. The change in the angular positions with stepper motor increments is shown in panel (b).

signal based on the computed FS topology of figure 9(a) is shown, where a semi-classical Boltzmann transport treatment was employed following Yagi [25]. A contour plot of the data from figure 7 (negative second derivative) is shown in figure 10(b), where it is clear to see that the FS topology expected from the band structure calculations cannot explain the vanishing of the AMRO oscillations along specific azimuthal directions. (In reference to figure 7(c), the progression from a finite to a vanishing oscillation period is evident). It is useful to compare the data with earlier results presented in figure 2 of [3] (in particular, the trace for  $\phi = 50^\circ$ ). For this angular region only one maximum is seen. Since SdH and dHvA oscillations are observed, there must be a closed FS of certain area, irrespective of the indications from the AMRO results for this direction.

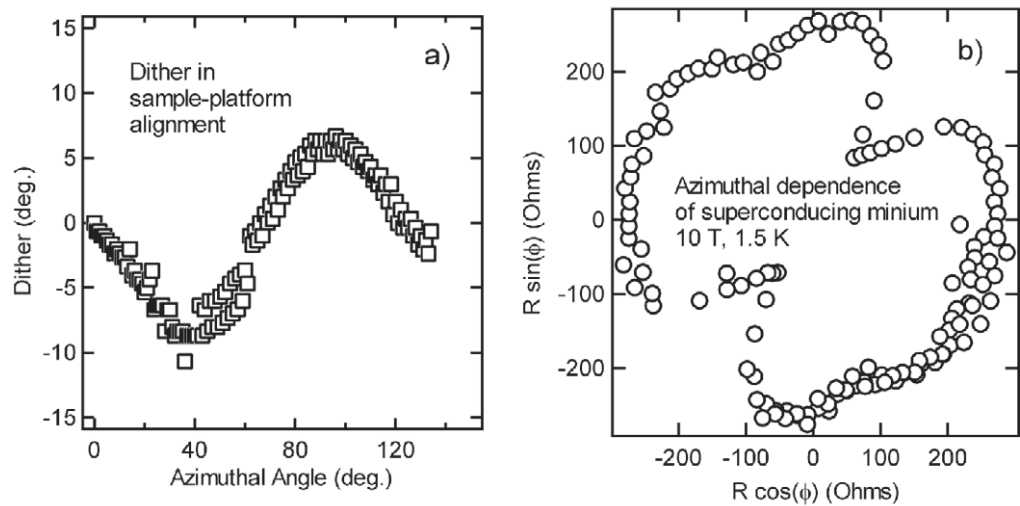


**Figure 8.** (a) Correction ('dither') for misalignment of the  $a$ - $b$  plane of the sample with the plane of the rotating platform. The dither is determined from the comparison of the digital stepper signal with the superconducting signature (for  $\theta$  modulo  $90^\circ$  when the field is exactly aligned in the  $a$ - $b$  plane). (b) Azimuthal dependence of MR in superconducting critical field region at 1.5 K and 10 T for precise  $B \parallel a$ - $b$  alignment.

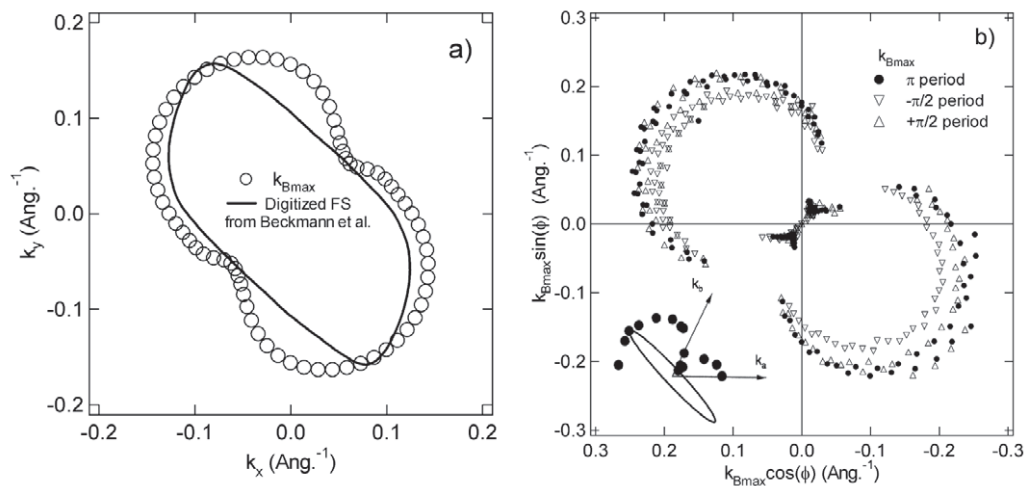


**Figure 9.** (a) Predicted  $k_{B \max}$  derived from the hole orbit FS topology from band structure calculations [2] using the geometrical construction [6]. (b)  $k_{B \max}(\phi)$  derived from the data in figure 7. The three data sets are for each cyclic interval  $\theta = \pi$ ,  $\theta = +\pi/2$ , and  $\theta = -\pi/2$  (due to the phase factor  $1/4$  in equation (1), a full Fourier transform of the  $\pi$  interval mixes the different  $\pm\pi/2$  periods slightly). The inset shows earlier results from [3] where the elliptical FS is derived from the geometric analysis of  $k_{B \max}(\phi)$ . The new more extensive results indicate that the semi-minor axis of the ellipse is too small to be defined in the central region.



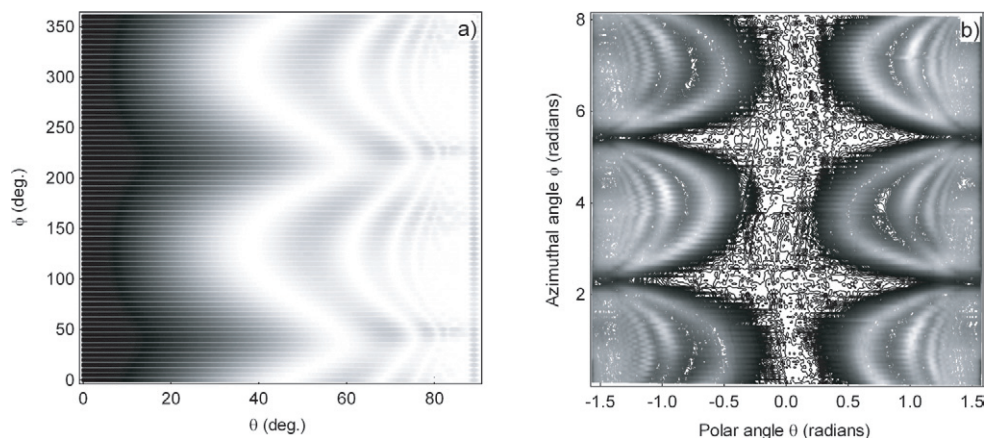


**Figure 10.** (a) Computed AMRO signal from Boltzmann theory using the computed FS in figure 9 (a). (b) Detailed contour representation of the negative second derivative of the AMRO signal  $A$  derived from the data of figure 7. Unlike the computed AMRO, the experimental AMRO period clearly vanishes for specific azimuthal rotation planes. (Note the different angular ranges for panels (a) and (b)).

### 2.3. AMRO in the superconducting critical region

In the third part of this investigation, the MR behaviour in the superconducting state was investigated in detail using a single angle rotator in a 9 T magnet (PPMS: Physical Property Measurement System, Quantum Design, San Diego, CA). Here the sample was rotated in the  $x$ - $y$  plane and the azimuthal dependence was not studied. (The plane of rotation was near the  $a$ - $c$  azimuthal direction). Representative data showing the interplane ( $R_{zz}$ ) MR anomaly are given in figure 11, where we note that the current direction is in all cases  $I \parallel c$ . At intermediate temperatures between  $T_c$  and  $T \rightarrow 0$  and a corresponding field range for  $0 < B \sim B_{c2}$ . The MR reaches a peak for  $B \parallel c$ . At higher fields the MR is negative, reaches a minimum, and then increases towards the SdH region (see figure 3(a)). For fields directed in-plane, i.e.  $B \parallel a$ - $b$ , there is neither a peak nor negative MR.

To explore in more detail the behaviour of the interplane resistance between the two limiting cases shown in figure 11, a set of systematic sample rotations were carried out for different temperatures and magnetic fields. Typical data are shown in figure 12(a). Here  $B \parallel a$ - $b$  coincides with  $\theta = 90^\circ$ . At 1.86 K, the sample is completely superconducting in this field direction until 9 T. Although the AMRO signal is quite evident in the data for rotations away from  $90^\circ$ , a peak in the MR not related to the AMRO appears near  $\pm 90^\circ$ . However, between 7 and 9 T, this peak disappears. At 3.4 K in figure 12(b), the AMRO are less apparent, and the superconducting and MR peak behaviour are more apparent. Again we note that between 5 and 9 T, the MR peak near  $\pm 90^\circ$  disappears. By plotting the same results versus the perpendicular and parallel field components  $B \parallel c = B \cos(\theta)$  and  $B \parallel a$ - $b = B \sin(\theta)$  respectively, the role of each becomes more apparent, as shown in figure 13 for three different temperatures. Comparing the same data sets at 3.4 K shown in figures 12(b) and 13, it is clear that the MR peak appears at a relatively constant value of  $B \parallel c$ , and that it then vanishes when  $B \parallel a$ - $b$  eventually starts to drive the sample normal. In figure 14, the relative height of the MR peak is compared with the

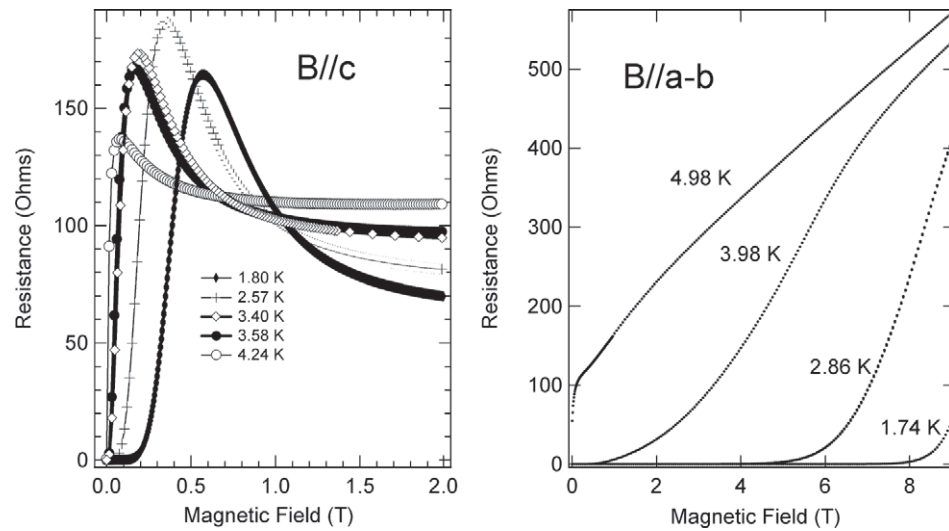


**Figure 11.** Interplane MR for  $B \parallel c$  and  $B \parallel a-b$  field orientations plane for  $\beta''$ -(BEDT-TTF) $_2$ SF $_5$ CH $_2$ CF $_2$ SO $_3$  at selected temperatures. For  $B \parallel c$ , the MR peak height is non-monotonic with temperature. For  $B \parallel a-b$ , there is no peak at any temperature.

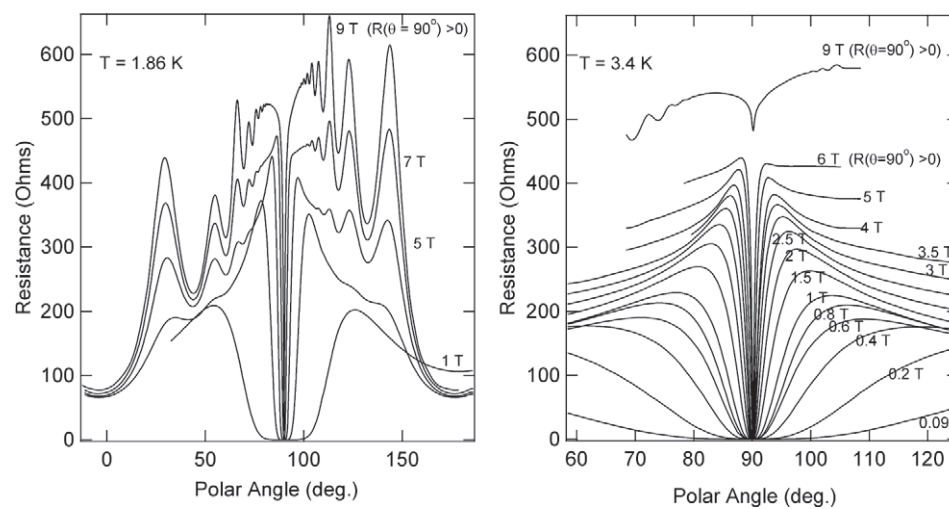


**Figure 12.** AMRO for  $\beta''$ -(BEDT-TTF) $_2$ SF $_5$ CH $_2$ CF $_2$ SO $_3$  for  $T = 1.86$  K (left-hand side panel) and  $T = 3.4$  K (right-hand side panel). For  $B \parallel a-b$  ( $\theta = 90^\circ$ ), a zero resistance state appears below 9 T at 1.86 K and below 6 T at 3.4 K. In the zero resistance state for  $B \parallel a-b$ , in fields tilted away from  $\pm 90^\circ$ , the MR shows a peak. When the  $B \parallel a-b$  resistance is no longer superconducting, the peak is attenuated. The oscillations at higher fields represent AMRO.



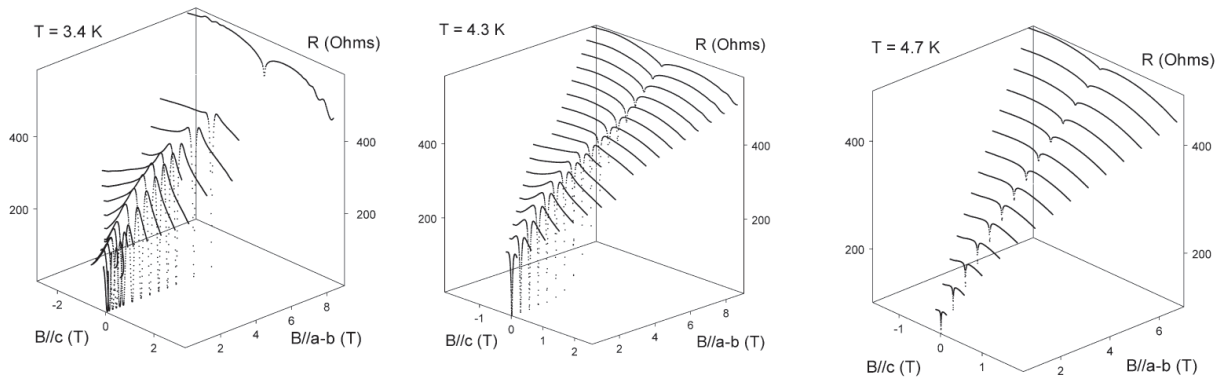


**Figure 13.** AMRO at 3.4, 4.3 and 4.7 K for increasing magnetic field  $B$  values. The data are plotted against the components of the field perpendicular to the layers,  $B \parallel a-b = B \cos(\theta)$ , and parallel to the layers,  $B \parallel a-b = B \sin(\theta)$ . For increasing temperature, the range of field over which the  $B \parallel a-b$  superconducting region decreases (as it does for the data for  $B \parallel a-b$  in figure 11). For  $B$  tilted away from the  $a-b$  plane, a finite component of  $B \parallel c$  appears, and when the sample is superconducting for  $B \parallel a-b$ , there is a corresponding peak in the MR.

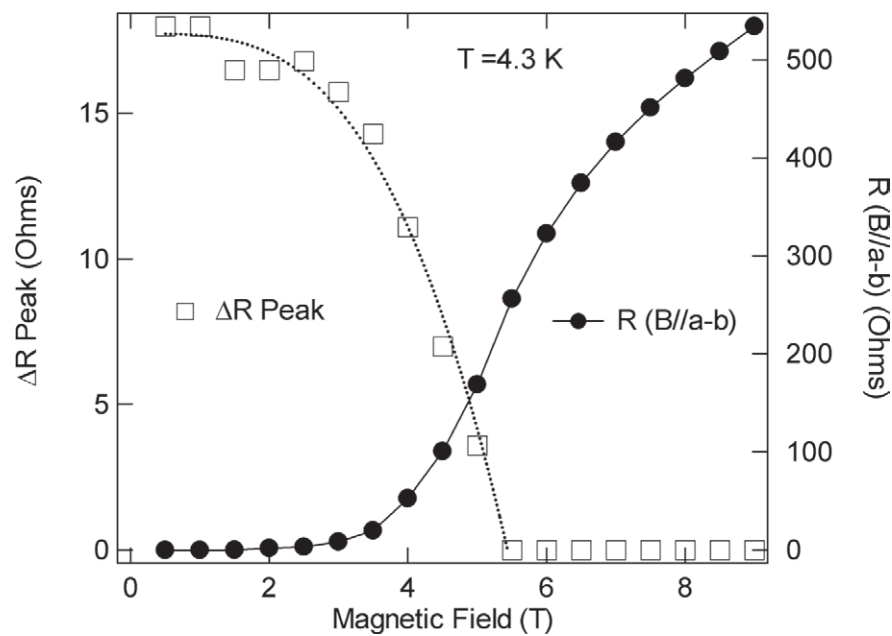


**Figure 14.** MR peak amplitude  $\Delta R \text{ Peak} = R(B \parallel c = 0.1 \text{ T}) - R(B \parallel c = 0.3 \text{ T})$  and MR minimum  $R(B \parallel c = 0)$  versus total magnetic field for rotation data in figure 13 for  $T = 4.3 \text{ K}$ .

in-plane resistivity for the 4.3 K data, and the correlation between the MR peak and the in-plane superconductivity is made more clearly. Referring again to figure 14, data for higher temperatures is again consistent with this picture.

In another MR rotation experiment, the MR peak phenomenon was investigated for two different azimuthal rotation planes, as shown in figure 15. Here data were taken at special angles

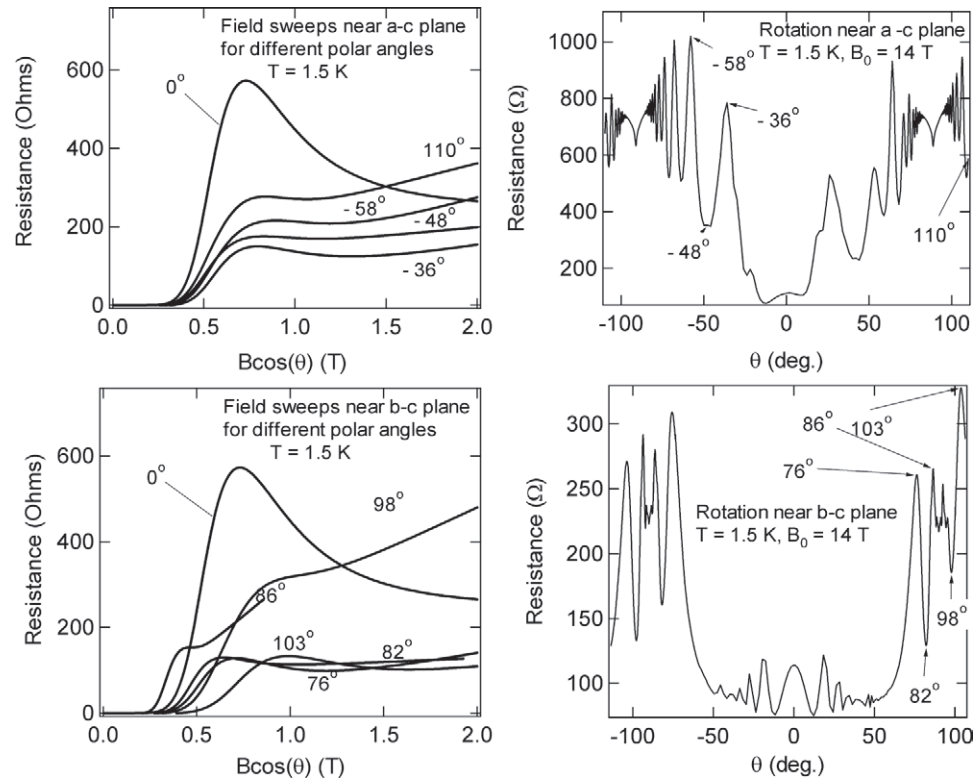


**Figure 15.** MR (left-hand side panels) taken at AMRO minima and maxima (right-hand side panels) for two different azimuthal rotation planes. The MR data are plotted versus  $B \parallel c$  to show the relation of the MR peak to the perpendicular field component. The data were taken by setting the rotation angles, and then sweeping the field from 0 to 14 T.

for both AMRO maxima and minima (see also [16]). For rotations near the  $a$ - $c$  plane, the correspondence of the peak with a nearly constant  $B \parallel c$  field component is consistent. However, for rotations near the  $b$ - $c$  plane where the AMRO features only appear near polar angles of  $90^\circ$  the MR peak location is more scattered with respect to a constant  $B \parallel c$  value. Although the uncertainties in  $B \cos(\theta)$  are larger near  $90^\circ$  for errors in  $\theta$ , the deviations in the peak positions from a constant  $B \parallel c$  component seemed to be outside the estimated errors.

In figure 16, we summarize the field and temperature-dependent parameters that are important to the MR of  $\beta''$ -(BEDT-TTF) $_2$ SF $_5$ CH $_2$ CF $_2$ SO $_3$ . Notably, the MR peak, plotted against the perpendicular field component (independently from finite parallel field), lies between the irreversibility line and thermodynamic critical field, and the MR minimum (also associated with the perpendicular field), lies near or just above the thermodynamic critical field.

The MR peak in the interplane resistance is common to a number of low dimensional systems including  $\kappa$ -(BEDT-TTF) $_2$ Cu(SCN) $_2$  [27]  $\kappa$ -(BEDT-TTF) $_2$ Cu[N(CN) $_2$ ]Br [14], and  $\beta$ -(BDA-TTF) $_2$ SbF $_6$  [28]. A general picture that leads to a model for this behaviour is one for a layered superconductor where the field and current are directed along the  $c$ -axis direction, perpendicular to the layers. Under these conditions, it is assumed that for sufficient interplanar spacing, pancake vortices exist in each layer, and there is no Lorentz-force related dissipation. Currents between layers can arise from two mechanisms. The first is by Josephson coupling

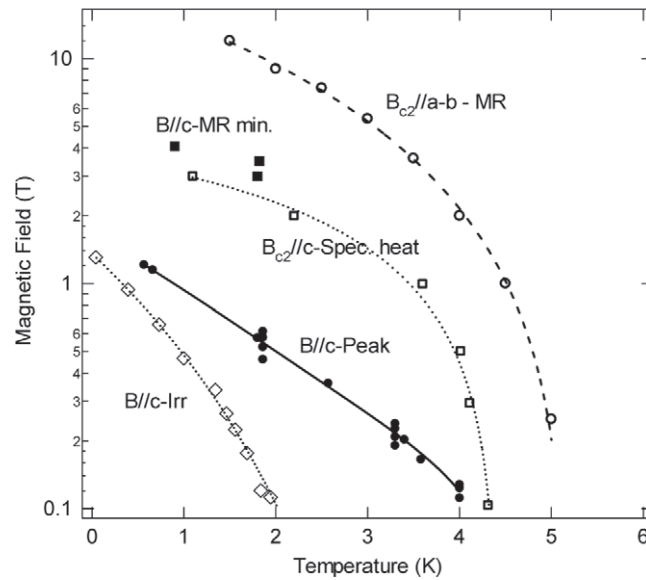


**Figure 16.** Summary of critical field behaviour for  $\beta''$ -(BEDT-TTF)<sub>2</sub>SF<sub>5</sub>CH<sub>2</sub>CF<sub>2</sub>SO<sub>3</sub>. The irreversibility line and the thermodynamic critical field are from magnetization and specific heat measurements respectively [26]. The loci of the field at the MR peak, the MR minimum, and the upper critical field for  $B \parallel a-b$  from MR are from the present study. Note that the MR peak is for the  $B \parallel c$  component of the magnetic field  $B \cos(\theta)$ . Lines are polynomial fits to the data.

of the vortices. Models for this coupling originate from earlier study on superconducting tunnel junctions. For a resistively shunted junction (RSJ), the junction conductance is  $Y_{\text{RSJ}}(T) = Y_{\text{N}} J_0^2 (\gamma(T)/2)$  where  $Y_{\text{N}}$  is the normal state conductance and  $J_0$  is the modified Bessel function.  $\gamma(T)$  is the Ambegaokar–Halperin parameter [29]  $\gamma = \hbar I_c(T)/ek_{\text{B}}T$ , where  $\gamma$  is the ratio of the Josephson coupling energy to the thermal energy, and  $I_c(T)$  is the Josephson critical current. For tunnel junctions, the critical current can be described by the Ambegaokar–Barotoff expression [30]  $I_c(T) = (\pi\Delta(T)/2eR_{\text{N}}) \tan h(\Delta(T)/2k_{\text{B}}T)$  where  $\Delta$  is the superconducting gap and  $R_{\text{N}}$  is the normal state resistance. The second contribution to the interlayer transport is the quasiparticle tunnelling  $Y_{\text{qp}}$ . Hence, the total conductance will be the sum of the two contributions, the superconducting pair conductivity  $Y_{\text{sp}}$  (see discussion below) and  $Y_{\text{qp}}$ ,  $Y_{\text{T}} = Y_{\text{sp}} + Y_{\text{qp}}$ . The essential feature of the model is that even in the presence of superconducting vortices, if the coupling is sufficiently weak due to fluctuations, the effective interplanar conductance can be even lower than in the normal state. This effect is enhanced by a reduction in the quasiparticle contribution to the conductivity due to the superconducting gap. Hence under these conditions, the conductivity (resistivity) can exhibit a dip (peak) in the intermediate range of temperature and/or magnetic field near the superconducting  $T$ – $B$  phase boundary.

The RSJ model has been applied to both cuprate superconductors and to organic conductors where the RSJ parameters depend on the system. The original model in [29] was applied to BiSCCO by Briceno *et al* [11] to explain the resistance peak in the interlayer resistivity in the critical region. Here the normal state resistance term  $1/Y_{\text{n}}$  term in the model was given by an empirical relation  $\rho_0 T^7 \exp(\Delta/k_{\text{B}}T)$ , and the critical current  $I_c(T)$  was modelled with

power law scaling behaviour for the current density where the total current was dependent on the vortex area, i.e.,  $I_c(T) \sim I_c(0)(1 - T/T_c)^{3/2}\phi_0/B$ . Gray and Kim [12] refined the model by considering the case of an *unshunted* junction to separate the purely junction pair contribution to the conductance  $Y_{sp}$  by subtracting  $Y_N$ , namely  $Y_p(T) = Y_N(J_0^2[\gamma(T)/2] - 1)$ . The application of the model to the organic superconductor  $\kappa$ -(BEDT-TTF)<sub>2</sub>Cu(SCN)<sub>2</sub> was first described by Friemel *et al* [13] who used the Gray and Kim [12] expression in combination with  $I_c(T, B)$  determined from experimental  $V(I)$  measurements where the field-dependent junction density was taken into account, and  $1/Y_{qp}$  in the form  $A + BT^2 + C \exp(\Delta(T)/k_B T)$ . This last expression represents the quasiparticle resistance in terms of metallic Fermi liquid behaviour in series with interplanar tunnelling due to the opening of the gap below  $T_c$ . A BCS expression for  $\Delta(T)$  was also used. With these assumptions, the MR peak at lower fields was satisfactorily fit to  $R_{zz}$  for  $\kappa$ -(BEDT-TTF)<sub>2</sub>Cu(SCN)<sub>2</sub> particularly in the lower field range where the vortex density is not too large. The failure of the model to fit the high field data has been noted more recently by Zuo and co-workers [10] who have examined the MR peak behaviour in both  $\kappa$ -(BEDT-TTF)<sub>2</sub>Cu[N(CN)<sub>2</sub>]Br [14] and  $\beta''$ -(BEDT-TTF)<sub>2</sub>SF<sub>5</sub>CH<sub>2</sub>CF<sub>2</sub>SO<sub>3</sub> [10]. The negative MR extends well beyond the peak field, and the models cannot yet explain this. To gain some insight into this problem, an overview of the characteristic magnetic field features from this study and others [26] is given in figure 16. As noted above, as long as the in-plane field is below the upper critical field line, a finite perpendicular field will produce a MR peak. Although the data are less extensive, the MR minimum appears to lie close to the thermodynamic critical field. If this is indeed the case, then the phenomena associated with the MR peak and negative MR lies within the superconducting state, except perhaps for some narrow fluctuation region at or above  $B_{c2}$ .

The main importance of our results is that even for large in-plane fields below  $B_{c2} \parallel a-b$ , the addition of a finite inter-planar field component will produce the MR peak effect. This result provides additional evidence for the validity of the model in terms of its origin in the Abrikosov vortex lattice that can only be produced by a  $B \parallel c$  field. The peak effect is correlated unambiguously with the presence of superconductivity. Hence it cannot arise purely from mechanisms such as interplane metal-insulator behaviour, magnetic scattering, etc. We also note that in previous study on  $\kappa$ -(BEDT-TTF)<sub>2</sub>Cu(SCN)<sub>2</sub>, the MR peak is suppressed very rapidly with uniaxial stress [31] applied perpendicular to the interplane direction, much more so than the suppression of  $H_{c2}$ . This is consistent with an increase in interplanar Josephson coupling, which would correspondingly reduce the junction resistance in the superconducting state.

### 3. Discussion and summary

We have presented specialized measurements of the interplane resistance of  $\beta''$ -(BEDT-TTF)<sub>2</sub>SF<sub>5</sub>CH<sub>2</sub>CF<sub>2</sub>SO<sub>3</sub> where some of the details of the electronic structure and superconducting properties have been explored. We now discuss our results in order of their presentation in section 2.

#### 3.1. Very high field measurements

It is clear that the very high field AMRO-type experiments reveal new regimes for this type of measurement. The appearance of very large SdH amplitudes in  $\beta''$ -(BEDT-TTF)<sub>2</sub>SF<sub>5</sub>CH<sub>2</sub>CF<sub>2</sub>SO<sub>3</sub> for large angles away from  $B \parallel c$  was very surprising. One possible origin of such an effect is that

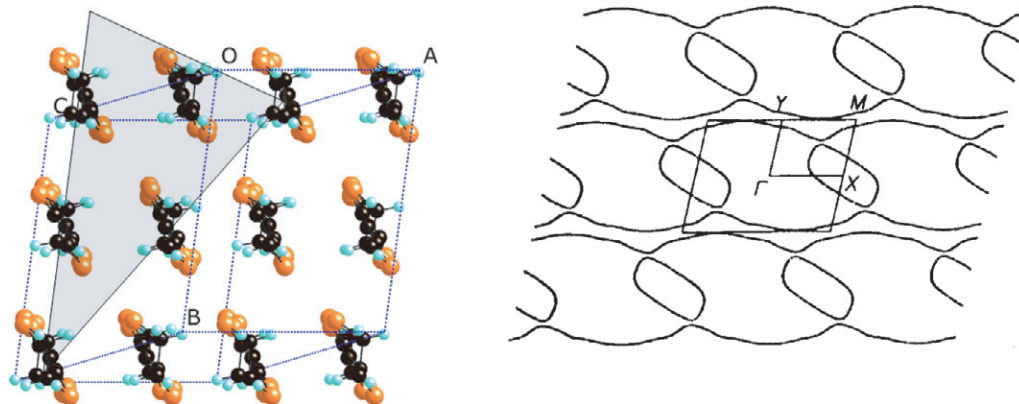


**Figure 17.** Summary of features correlated with azimuthal dependence (Figures after [1] and [2]). Left panel: Crystallographic region where the azimuthal rotation causes a large change in the  $\tan(\theta)$  period and a minimum in the MR and the superconducting dip resistance. Right panel: corresponding FS topology.

due to some as of yet undetermined warping, the Landau level energies and the Fermi energies were in coincidence at high angles of order  $60^\circ$  away from  $B \parallel c$ . Although not in tilted fields, similar effects have been reported in  $\beta$ -(BEDT-TTF) $_2$ I $_3$  [32]. Clearly, systematic studies versus both  $\theta$  and  $\phi$  in the 45 T range would be very informative in revealing more detailed aspects of the 3D FS topology, in combination with a more complete treatment of the Lifshitz–Kosevich damping factors and the effects of the background AMRO and MR.

### 3.2. Highly systematic AMRO studies

An automated two angle rotator also produced detailed information at lower fields where measurements versus  $\theta$  and  $\phi$ , confirmed previous assertions that the ARMO study for  $\beta'$ -(BEDT-TTF) $_2$ SF $_5$ CH $_2$ CF $_2$ SO $_3$  reveals a highly elliptical closed orbit, in disagreement with the band structure predictions. Moreover, in measurements where the sample was continuously rotated in field through the  $b$ – $c$  region it is clear that there is a sharp change (increase) in the  $\tan(\theta)$  period. Hence even the width of the semi-minor axis of the FS ellipse is uncertain. The region where the rapid change in behaviour occurs is correlated with the real crystal structure as shown in figure 17. It is possible that the open orbit band contributes in some unknown way to the AMRO signal, or that the cylindrical FS is warped, also in some unknown manner. It is important to note that in all of our AMRO measurements on the sample describe herein, we have not observed the ‘coherence peak’ at  $B \parallel a$ – $b$  for any azimuthal angle in the normal state. This is consistent with previous, comparative studies [33] where for some organic superconductors such as  $\kappa$ -(BEDT-TTF) $_2$ I $_3$ , this feature is observed, but not in the case of  $\beta'$ -(BEDT-TTF) $_2$ SF $_5$ CH $_2$ CF $_2$ SO $_3$ . The absence of this peak is an indication of incoherent interlayer transport [34, 35], and this may also be a factor in the unusual behaviour of the AMRO. The systematic rotation study also produced detailed azimuthal in-plane information about the MR in the vicinity of the superconducting transition as shown in figure 8(b). It is interesting to note that the azimuthal region where the MR( $\phi$ ) has a minimum, indicating a higher critical field, is the same region where the  $\tan(\theta)$  period changes dramatically. Figure 8(b) also shows additional symmetrical features in the MR( $\phi$ ) data that are correlated with the crystal structure, and further study at different fields in the



critical field region where the resistance is not zero would be very useful to better map out these symmetries for comparison with the electronic and physical structure of the compound.

### 3.3. Interplane transport in the superconducting critical region

The MR peak in the interplanar resistance that appears in a number of layered superconducting compounds has proved to be a rich source of new physics. The main results of this study, at least for the compound  $\beta''$ -(BEDT-TTF)<sub>2</sub>SF<sub>5</sub>CH<sub>2</sub>CF<sub>2</sub>SO<sub>3</sub>, are that: (i) the MR peak depends primarily on the perpendicular field component  $B \parallel c$ ; (ii) the MR peak will appear for finite  $B \parallel c$  as long as the sample is superconducting when  $B \parallel a-b$  is below  $B_{c2} \parallel a-b$ ; (iii) the MR peak is unambiguously correlated with the superconducting state, and even the MR minimum which appears at higher fields, is limited by the thermodynamic critical field for  $B \parallel c$ . (It is noteworthy that the absence of the ‘coherence peak’ discussed above as evidence for incoherent interlayer transport is not a necessary condition to observe the MR peak, since for  $\beta$ -(BDA-TTP)<sub>2</sub>SbF<sub>6</sub> [28] and  $\kappa$ -(BEDT-TTF)<sub>2</sub>Cu(SCN)<sub>2</sub> [36] both the coherence and MR peaks appear). Although the models based on the RSJ concept can fit the data for different materials, the fitting parameters can be unrealistic, and the high field agreement is not possible in any case. Future study will be needed, in light of figure 14, to properly treat the critical region at high fields. Also, in the present study, we note that for substantial in-plane fields below the upper in-plane critical field, the MR peak shows deviations from purely perpendicular  $B \parallel c$  field behaviour. This is evident in the slight curvature of the MR peak positions in figure 13 with respect to the  $B \parallel c - B \parallel a-b$  plane, and also in the data shown in the lower panel of figure 15, where most of the data is at very high tilt angles and therefore high in-plane fields approaching 14 T. Since the in-plane field can produce Josephson vortices, and since for  $I \parallel c$  a Lorentz force is possible for tilted samples, other effects must come into play at some point.

## 4. Conclusions

Our study shows that advanced instrumentation combined with highly systematic measurements at high magnetic fields and low temperatures will yield new information about materials. We have presented new measurements on the completely organic superconductor  $\beta''$ -(BEDT-TTF)<sub>2</sub>SF<sub>5</sub>CH<sub>2</sub>CF<sub>2</sub>SO<sub>3</sub> in high magnetic fields and also in highly systematic angular-dependent studies. Although the general behaviour of the MR follows the standard behaviour observed in the general class of organic materials with a quasi-2D hole orbit, our investigation shows that in essence, the tight binding band structure prediction for the FS topology associated with the closed orbit cannot explain the data, particularly when the field is directed in the vicinity of the  $b-c$  plane. In this region, the three properties: SdH amplitudes;  $\tan(\theta)$  period, and superconducting critical field, all show significant deviations from a conventional elliptical description of the hole orbit topology. Likewise, for  $B \parallel c$  as in figure 3(b), there is no evidence (i.e. a ‘coherence peak’) for coherent interplane transport, and to date, no direct evidence for the 1D band has been forthcoming. To determine the origin of this behaviour, two possibilities arise, namely the unique nature of the completely organic, low symmetry anion SF<sub>5</sub>CH<sub>2</sub>CF<sub>2</sub>SO<sub>3</sub><sup>-</sup>, and/or the role of the open orbits in the physical properties, particularly at strategic field directions where the unconventional properties appear. Finally, we have been able to strengthen the correlation of the anomalous MR peak seen in the superconducting critical field region with the appearance of Abrikosov vortices induced by perpendicular fields, even in the presence of much larger

in-plane fields, as long as the latter is below the upper critical field. Hence this MR peak cannot arise from non-superconducting mechanisms involving  $R_{zz}$ , such as interplane incoherence and metal-insulating behaviour.

Although the present and previous investigations of this material represent a significant effort, as described above there are many mysteries, and opportunities, awaiting future researchers in this area. As very high field magnets, both dc and long-pulse systems, become more accessible, truly systematic studies (versus  $T$ ,  $P$ ,  $\theta$ ,  $\phi$ , etc) to follow up on measurements as in figures 3 and 7 will be more practical. Since more subtle features in AMRO signals are enhanced at higher fields, many of the mysteries may finally be addressed.

### Acknowledgments

This study was initiated with support from NSF-DMR 09-71714, and was further carried out under NSF-DMR 02-03532 and completed under NSF-DMR 06-02859. Work at Argonne National Laboratory was supported by the Office of Basic Energy Sciences, Division of Materials Sciences of the US Department of Energy under contract W-31-109-ENG-38. Work at Portland State University was supported by NSF CHE-9904316. We thank D Graf, E S Choi, K Storr, T Murphy, E Palm, R Mizutani, T Kinoshita, C Terakura and the respective staffs of the NHFML, NIMS, and NRI for assistance in carrying out the work describe herein. We are also grateful to O Drozdova of IMS for x-ray characterization of the sample.

### References

- [1] Geiser U *et al* 1996 *J. Am. Chem. Soc.* **118** 9996
- [2] Beckmann D, Wanka S, Wosnitza J, Schlueter J A, Williams J M, Nixon P G, Winter R W, Gard G L, Ren J and Whangbo M-H 1998 *Eur. Phys. J. B* **1** 295
- [3] Wosnitza J *et al* 1999 *Synth. Met.* **103** 2000
- [4] Kajita K, Nishino Y, Takahashi T, Kato R, Kobayashi H, Sasaki W, Kobayashi A and Iye Y 1989 *Solid State Commun.* **70** 1189
- [5] Kartsovnik M V, Laukhin V N, Pesotskii S I, Schegolev I F and Yakovenko V M 1990 *J. Phys. I* **2** 89
- [6] Peschansky V G, Lopez J A R and Yao T G 1991 *J. Phys. I France* **1** 1469
- [7] Wosnitza J *et al* 2001 *Phys. Rev. Lett.* **86** 508
- [8] Zuo F, Su X, Zhang P, Brooks J S, Wosnitza J, Schlueter J A, Williams J M, Nixon P G, Winter R W and Gard G L 2000 *Phys. Rev. B* **60** 6296
- [9] Nam M-S, Ardavan A, Symington J A, Singleton J, Harrison N, Mielke C H, Schlueter J A, Winter R W and Gard G L 2001 *Phys. Rev. Lett.* **87** 117001
- [10] Su X, Zuo F, Schlueter J A, Williams J M, Nixon P G, Winter R W and Gard G L 1999 *Phys. Rev. B* **59** 4376
- [11] Briceno G, Crommie M F and Zettl A 1991 *Phys. Rev. Lett.* **66** 2164
- [12] Gray K E and Kim D H 1993 *Phys. Rev. Lett.* **70** 1693
- [13] Friemel S, Pasquier C and Jerome D 1997 *Physica C* **292** 273
- [14] Zuo F, Schlueter J A and Williams J M 1999 *Phys. Rev. B* **60** 574
- [15] Yamaji K 1989 *J. Phys. Soc. Japan* **58** 1520
- [16] Brooks J S *et al* 2002 *Mol. Cryst. Liq. Cryst.* **380** 109
- [17] Bird M D, Bole S, Dixon I, Eyssa Y M, Gao G J and Schneider-Muntau H J 2001 *Physica B* **294-5** 639
- [18] Dixon I R, Bird M D and Bole S 2002 *IEEE Trans. Appl. Supercond.* **12** 452-55
- [19] Miller J R 2003 *IEEE Trans. Appl. Supercon.* **13** 1385
- [20] Stepankin V 1995 *Physica B: Condens. Matter* **211** 345



- [21] Brooks J S, Fisk Z, Hill S, Sarrao J, Szabo T, Uji S, Sandhu P, Valfells S and Seger L D 1996 *Int. Workshop on High Magnetic Fields: Industry, Materials and Technology, Tallahassee (28 February–1 March 1996)* (Singapore: World Scientific) p 30
- [22] Shoenberg D 1994 *Magnetic Oscillations in Metals* (Cambridge: Cambridge University Press)
- [23] Kartsovnik M V, Laukhin V N, Pesotskii S I, Schegolev I F and Yakovenko V M 1991 *J. Phys. I France* **2** 89
- [24] House A A, Harrison H, Blundell S J, Deckers I, Singleton J, Herlach F, Hayes W, Perenboom J A A J, Kurmoo M and Day P 1996 *Phys. Rev. B* **53** 9127
- [25] Yagi R 1992 *Thesis* University of Tokyo
- [26] Wanka S, Hagel J, Beckmann D, Wosnitza J, Schlueter J A, Williams J M, Nixon P G, Winter R W and Gard G L 1998 *Phys. Rev. B* **57** 3084
- [27] Zuo F, Schlueter J A, Kelly M E and Williams J M 1996 *Phys. Rev. B* **54** 11973
- [28] Choi E S, Jobilong E, Wade A, Goetz E, Brooks J S, Yamada J and Tokumoto M 2003 *Phys. Rev. B* **67** 174511
- [29] Ambegaokar V and Halperin B I 1969 *Phys. Rev. Lett.* **22** 1364
- [30] Ambegaokar V and Baratoff A 1963 *Phys. Rev. Lett.* **10** 486
- [31] Choi E S, Brooks J S, Han S Y, Balicas L and Qualls J S 2001 *Phil. Mag. B* **81** 399
- [32] Kang W, Montambaux G, Cooper J R, Jerome D, Batail P and Lenoir C 2989 *Phys. Rev. Lett.* **62** 2559
- [33] Wosnitza J 2002 *Phys. Rev. B* **65** 180506
- [34] McKenzie R H and Moses P 1998 *Phys. Rev. Lett.* **81** 4492
- [35] Moses P and McKenzie R H 1999 *Phys. Rev. B* **60** 7998
- [36] Singleton J, Goddard P A, Ardavan A, Harrison N, Blundell S J, Schlueter J A and Kini A M 2002 *Phys. Rev. Lett.* **88** 037001